Towards Artificial Ossification for Bone-inspired Technical Structures

R.Starke & I. Vukorep
Chair of Digital Design Department, BTU Cottbus-Senftenberg, Germany, starke@b-tu.de, ilija.vukorep@b-tu.de

K. Frommelt
DFG Research Training Group 1913, BTU Cottbus-Senftenberg, Germany, konrad.frommelt@b-tu.de

A. Melcher
Institute of Geometry at Faculty of Mathematics, Dresden University of Technology, Germany, alexander.melcher@tu-dresden.de

T. Hinze
Department of Bioinformatics, Friedrich Schiller University Jena, Germany, thomas.hinze@uni-jena.de

ABSTRACT: Since its first description in 1892, the adaptation of internal bone structure to changing loading conditions over time, known as Wolff's Law, has inspired a wide range of research and imitation. This investigation presents a new bone-inspired algorithm, intended for the structural design of technical structures and capable of optimizing the shape and size of three-dimensional lattice structures. Unlike conventional structural optimization methods, it uses interacting artificial agents that closely follow the cellular behaviour of the biological blueprint. Agents iteratively move, alter cross-sections, and reposition axes in the latticework. The efficacy of the algorithm is tested and evaluated in two case studies. This agent-based approach lays the theoretical foundation for an implementation of adaptive structural building components and provides a tool for further research into the spatial aspects of natural ossification.

1 INTRODUCTION

1.1 *Natural Ossification*

Ossification is a biological process that constantly remodels bone structure in reaction to the applied loads. This process was first described in *The Law of Bone Remodelling* (Wolff, 1892) and shows for instance in the bone resorption experienced by astronauts. By this process, the bone's balance between stability and material usage is permanently adjusted during its lifetime. Tube bones in mammal skeletons, like femur or humerus, consist of an outer shell, the cortical bone, and a porous inner framework, the trabecular bone. The simulation of this porous framework's adaptability is at the core of this research. There are two main agents essential for its adaptability: *osteoblast* cells, which mineralise and strengthen bone tissue in areas of high stress, and *osteoclast* cells, which demineralise and remove tissue in areas of low stress. The tissue consists of ossein fibres, a kind of collagen with high strength and elasticity. Existing biological simulations of osteoblasts and osteoclasts, called co-culture systems (Safadi et al., 2009), mainly focus on the correct simulation cytochemistry and collagen fibre array on a molecular level. The proposed method's novelty lies in the focus on spatial relations and results for building scales. Downward from the 6th level of organisation, the trabecular architecture, visible to the naked eye, described in *The Material Bone: Structure-Mechanical Function Relations* (Weiner and Wagner, 1998), the cellular and molecular processes are meaningfully translated into abstract spatial operations. The result is a new lightweight shape and size optimisation algorithm that dynamically visualises ossification principles, including osteoblast and osteoclast movement.

1.1 *Bionics*

The analysis and adaptation of biological processes and structures have inspired optimisation methodologies in structural engineering for many decades. For the development of serially produced structures, but especially in automotive and aerospace engineering (Cavazzuti et al.,

2011), the creation of lightweight and highly efficient parts is often paramount. Efficiency in this context may be quantified by various metrics, e.g., load capacity, robustness, fatigue tolerance, or manufacturing cost. Bionics also had a considerable impact on our built environment (Januszkiewicz and Banachowicz, 2017), which can be expected to further increase with the advent of fabrication technologies like additive manufacturing, making design spaces of finely graded and highly optimised parts affordable to the public. Structural optimisation includes different methodological approaches: topology optimisation, shape optimisation, size optimisation, and material optimisation. While the proposed algorithm utilises the finite element method (FEM) (Hughes, 1987), it is not used for the topology optimisation as in the Soft-Kill-Option (SKO) method (Baumgartner et al., 1992) or a direct optimisation of trabecular architecture (Jang et al., 2008; Boyle et al., 2011). Instead, an initial trabecular architecture is calculated with FEM, and the resultant forces are further processed as stimuli for artificial osteoblasts and osteoclasts. This process adheres much closer to natural ossification than conventional structural optimisation solutions. The agent-based approach was first introduced as a pure size optimisation method (Melcher et al., 2019) in Grasshopper3d. Based on this approach, a new agent-based algorithm was written in Python for this investigation. It is accomplishing, among other improvements, the implementation of shape optimisation and the reduction of computation time by two orders of magnitude.

2   METHOD

2.1 Algorithm Structure

To translate the underlying biochemical processes of ossification into an algorithm of geometrical transformations, several abstractions had to be made. Naturally, the chosen abstractions aim to match the effects of natural ossification as closely as possible, taking into account that this investigation tries to use the principles of natural ossification for technical structures of a much larger scale. The proposed algorithm works by gradually optimising an initial structure. The topology and density of the initial structure are determined a priori, meaning any setup of two- or three-dimensional lattice structure, including supports and loads, may be supplied to the algorithm. In natural ossification, the remodelling through osteoblasts and osteoclasts leads to two effects: an increase or decrease of cross-sectional area and the gradual shift of the filament axis when the material is added or removed asymmetrically to the cross-section, effectively changing the structural geometry. The slow lateral shift of the filaments can be imagined roughly similar to the formation of dripstone. In the algorithm, this process is simplified and repeated for a defined number of steps. Each iteration is made up of the following subsequent steps: The structural calculation of internal forces (Figure 1), the repositioning of agents (Figure 2b), the alteration of the beam diameter, and the repositioning of beam axes (Figure 3). It is assumed that filament cross-sections are always circular and that single beams will remain straight during the process. Cylindrical elements are proven to be able to simulate the load bearing of the sometimes plate-like trabecular bone structure accurately (Lenthe et al., 2006).
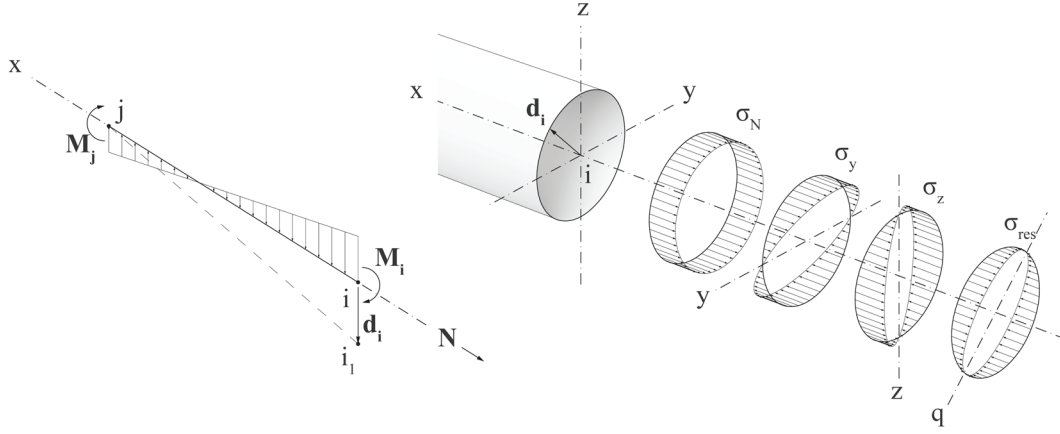
Figure 1. a: Beam between nodes i and j with normal forces N, and bending moments $\boldsymbol{M_i}$ and $\boldsymbol{M_j}$ and potential repositioned node i_1. b: Beam cross-section with stress distribution σ_y, σ_z , and σ_N resulting from $\boldsymbol{M_i}$, $\boldsymbol{M_j}$, and N; resulting stresses σ_{res} with neutral axis q.

For each step, the internal forces in the model are calculated at predefined probe points, equally dividing the beams. First the vectors $\boldsymbol{M_i}$, $\boldsymbol{M_j}$, and $\boldsymbol{N}$ are calculated by the FEM (Figure 1a), a linear system of equations is set up and numerically solved for each connection point of beams and for each load entry point according to the mechanical equilibrium, as in the method by *Melcher et al*. Thus, the normal forces N and bending moments M_y and M_z can be retrieved as scalars for each probe point individually (Figure 1b), while shear and torsion forces are ignored in this model. These lead to stress distributions that are superpositioned into a resulting stress distribution σ_{res}. For evaluation and optimization of the model, a single-value equivalent stress σ_e is used. For circular cross-sections, σ_e derives from

$$\sigma_e = \sigma_N + \frac{M_{res}}{W} \tag{1}$$

with

$$\sigma_N = \frac{N}{A} = \frac{N}{\pi \cdot r^2} \; ; \; M_{res} = \sqrt{M_y^2 + M_z^2} \quad \text{and } W = \frac{\pi \cdot d^3}{32} \tag{2;3;4}$$

The equivalent resulting stress is:

$$\sigma_e = \frac{N}{\pi \cdot r^2} + \frac{\sqrt{M_y^2 + M_z^2} \cdot 32}{\pi \cdot d^3} \tag{5}$$

In each iteration, the agents are evaluating the set of equivalent stresses in a range predefined by the vision radius r_{vis} (Figure 2b). Osteoblasts will move toward the point P_{tmax} of highest absolute stresses $max.|\sigma_e|$, while osteoclasts will target the point P_{tmin} of the lowest absolute stresses moving at a constant rate $\boldsymbol{v_{step}}$

$$\boldsymbol{v_{step}} = \boldsymbol{v_{total}} \cdot \frac{a}{|v_{total}|} \tag{6}$$

where a = velocity factor; $\boldsymbol{v_{total}}$ = vector between agent position and P_{tmax} or P_{tmin}

An agent can only affect one probe point within its effect radius r_{eff}. With the vision radius larger than the effect radius, agents will travel to distant target points while affecting points in the closer vicinity. Radii are changed by the effect strength, a numerical parameter set at the beginning of the optimisation. Cross-section areas with higher stress levels will be extended, while those with low stress levels will be reduced accordingly.

In the following step, the agent will initiate a lateral displacement of the beam axis x (Figure 1). To approximate the gradual shifting effect, the beam axis is rotated. To do this, the agent first checks on which side of the corresponding axis it is located and sets the center of rotation to the opposite end. In the beam subjected to moment forces M_{res}, the resulting stresses are unevenly distributed around the cross-section with the pivot axis q. A lateral movement of the beam axis to the side of the highest real stresses, i.e. the smallest tensional stress or the largest compression stress, is preferable from a structural point of view due to the reduction of the ideal lever of internal moment forces. The direction of the transformation $\boldsymbol{d_i}$ is therefore set opposite to the moment force M_{res} at the current position, while the amplitude is the product of M_{res} and a predefined global shift factor. To keep the structural integrity of the model at node points, a new node i_e is interpolated between the displaced vertices of all connected beams (Figure 3)

$$i_e = \frac{\sum_{k=1}^{n} P_k}{n} \tag{7}$$

where P_k = beam vertices connected at node i; n = number of beam vertices connected at node i

The beams are then rebuild from the new vertices. After that, a new cycle begins.
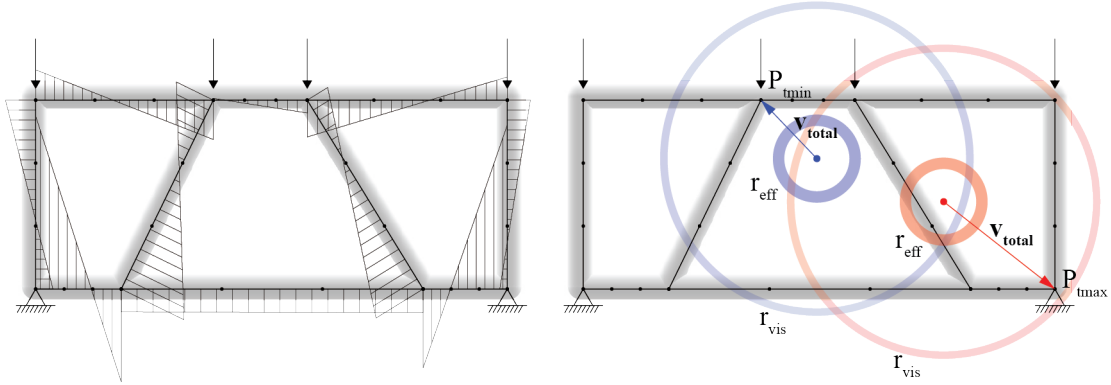
2.2 Implementation

Figure 2. Case study 1. a: two-dimensional lattice structure with loads, supports, and resulting bending moments M_{res}. b: Osteoblast, in red, and osteoclast, in blue, with effect radius and vision radius.
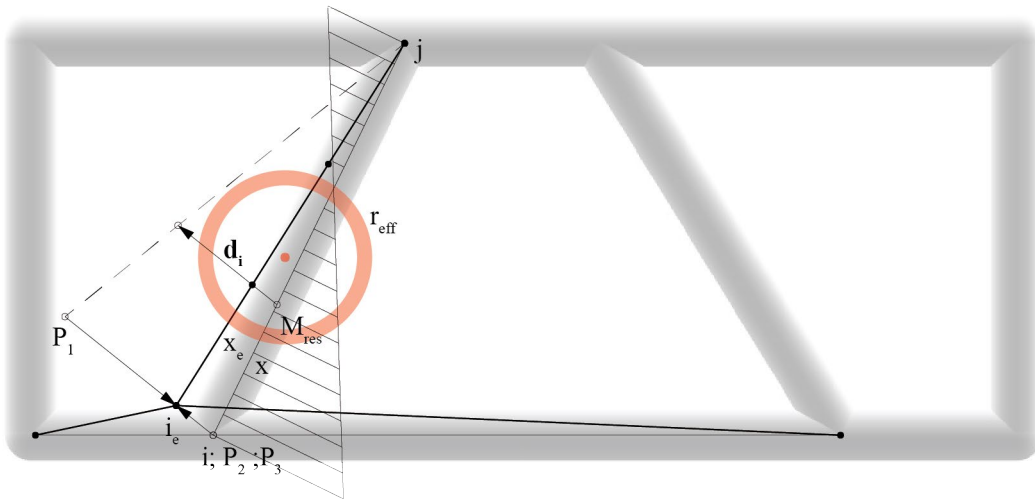

Figure 3. Case study 1. Vertex P_1 moved according to $\boldsymbol{d_i}$. New node i_e interpolated from beam vertices P_1, P_2 and P_3. New axis x_e build from nodes j and i_e.

Case study 1 represents a simple two-dimensional structure to verify and visualise the proposed algorithm (Figure 2). Based on Voronoi diagrams, the model contains 10 beams arranged in a four-sided rectangular frame with an inner lattice structure created by natural neighbour interpolation. All beams are connected without articulations. Loads are applied as point loads to the four uppermost vertices of the frame. The supports at the vertices of the bottom corners have no degree of freedom. The result is a simple yet statically indeterminate structure calculated with FEM provided by the Karamba3d implementation to GhPython (Preisinger, 2013). The predefined number of agents is generated at random positions throughout the given frame. In a second step, a more extensive 3-dimensional model with 92 beams was used (Figure 5), with loads and support conditions analogous to the first case study.

The arguments listed in Table 1 must be specified for the algorithm to work the model. Optionally they can be set proportionally to the size of the total frame for easier use.

Table 1. Parameters of the Case Studies

Parameters	Case Study 1	Case Study 2
iterations*	1000	500
model diameter [m]	3.32	33.17
beams	10	92
pointloads[kN]	100	100
probe points per beam*	4	4
beam axis shift factor*	0.1	0.15
initial beam radius[cm]*	8	26
minimal beam radius threshold[cm]*	3.3	5.2
number of osteoblasts*	1	20
number of osteoclasts*	1	20
cluster limit*	-	1
vision radius of the agents, r_{vis}[m]*	1	6.5
effect radius of the agents, r_{eff}[m]*	0.25	1.8
velocity factor, a*	0.1	0.65
effect strength of the agents[cm]*	0.1	0.25
computation time[s]**	22	128

* Obligatory initialization Arguments for the Algorithm, aside from lattice structure, loads and supports.
** GhPython on Intel(R) Core(™) i7-10875H, GeForce RTX 2070 with Max-Q, 32GB RAM

2.3 Limitations

Some difficulties were encountered in the spatial abstraction of the natural processes. Additional restraints to the target function were set up to prevent overshooting of target points by the agents and clustering of agents. Additionally, osteoclasts had to be prevented from targeting probe points with a radius below a minimum threshold. The reduction of beam radii to 0 happens in natural ossification and leads to the effective elimination of trabeculae and a change in topology. This natural elimination process was intentionally excluded at this stage of the research. The node points connecting multiple beams had to be equalised for the lowest local comparison stress and the highest radius, respectively, to prevent osteoblasts and osteoclasts from getting locked into a 'tug of war' over different beams vertices incorporated in the same node. This equalisation process is executed once per connected node in each cycle.

The proposed movement mechanics are an approximation of the natural osteoblast and osteoclast migration. How exactly mechanical forces are translated into stimuli for bone remodelling is still debated in the scientific community. Micro-cracks in the bone tissue, trapped osteocytes, bone morphogenetic proteins (Khurana et al., 2010), and chemotaxis (Thiel et al., 2018) are presumed to have an influence.

In natural bone remodelling, osteoblasts and osteoclasts are confined to move along the surface of the trabecular bone. While technically possible, the calculation of movement on a surface would multiply the computation time without a substantial improvement to the optimisation. Therefore, this investigation allows unconstrained agent movement throughout the frame and represents the beam shape only by a numerical value for the radius of circular cross-sections. Thus, the whole model can be represented only by numbers, points, and lines. For the calculation

of internal forces, beam radii are ignored. They are used only after the last iteration for visualising the beam volumes.

3   RESULTS

After the conclusion of the iterative process, both models experience significant changes in geometry. The repositioning of beam axes leads to orientations approaching an ideal line of thrust. For the simple two-dimensional model, the resulting structure resembles a strut-frame truss(Figure 4), which intuitively confirms the ability of the algorithm to create a more efficient structure. In the 3-dimensional model, the resulting beam geometry resembles a bowstring arch bridge, but can as well be compared with the trajectories for compression and tension that can be observed in a solid beam. The resulting geometry reduces moment forces by approximation of an ideal equilibrium network made up of funicular lines, a two- or three-dimensional geometry creating an equilibrium between loads and support conditions with only normal forces in the edges (Block et al., 2017; Block, 2009).
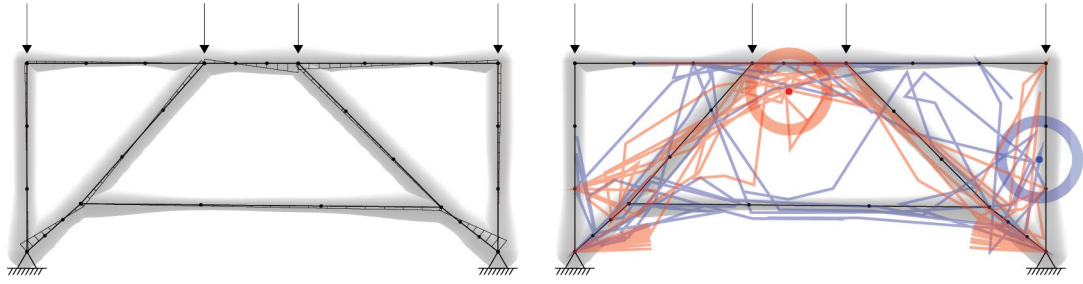

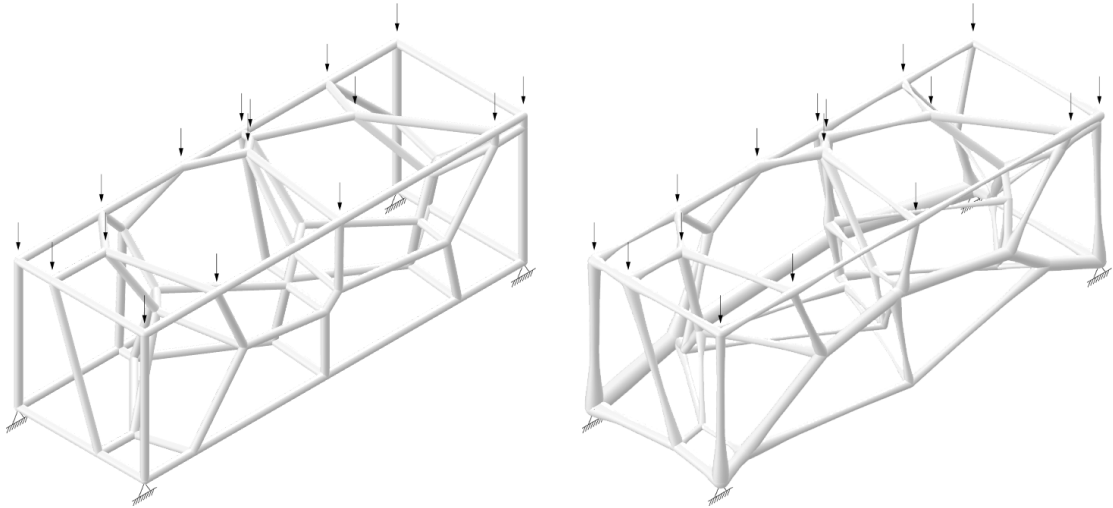Figure 4. Case Study 1. a: reduced moments of optimised model. b: agents movement paths.

Figure 5. Case study 2. a: initial model. b: optimised model.

An apparent reduction of comparison stress throughout the model of case study 1 after 1000 iterations is evident (Figure 6a). The average comparison stress was reduced from 2.62 kN/cm² in the benchmark structure with uniform radii to 0.54 kN/cm² in the optimised structure. More importantly, the standard deviation of the comparison stress was reduced from 2.38 kN/cm² to 0.05 kN/cm², clearly indicating a more equal distribution of stress. The radius alterations cause those improvements according to the local forces, which results in a less equal distribution of radii (Figure 6b). The average bending moment force reduction at the probe points from 6.72 kNm to 0.60 kNm is independent of the cross-section and solely caused by the axis alteration.

The sum of beam volumes stayed roughly constant during the optimisation, starting at 0.25m³, finishing at 0.29m³. Since, unlike in natural ossification, the agent strength is equal for osteoblasts and osteoclasts, the increase of total volume by 16% might be caused by the node point equalisation of all the connected beam endpoints towards the highest radius, de facto multiplying the strength of agents when altering node points. The gradual improvement of geometry to minimise bending moments marks a qualitative improvement of the method introduced by (Melcher et al., 2019). The platform change from grasshopper to Python yields a 334 times faster computation for a two-dimensional structure with 94 beams and similar initialisation parameters, computed on the same hardware (Table 1).

The described patterns in the distribution of stress and moment forces are similar in the second case study (Figure 5, Figure 7), proving the method veritable for three-dimensional structures as well.
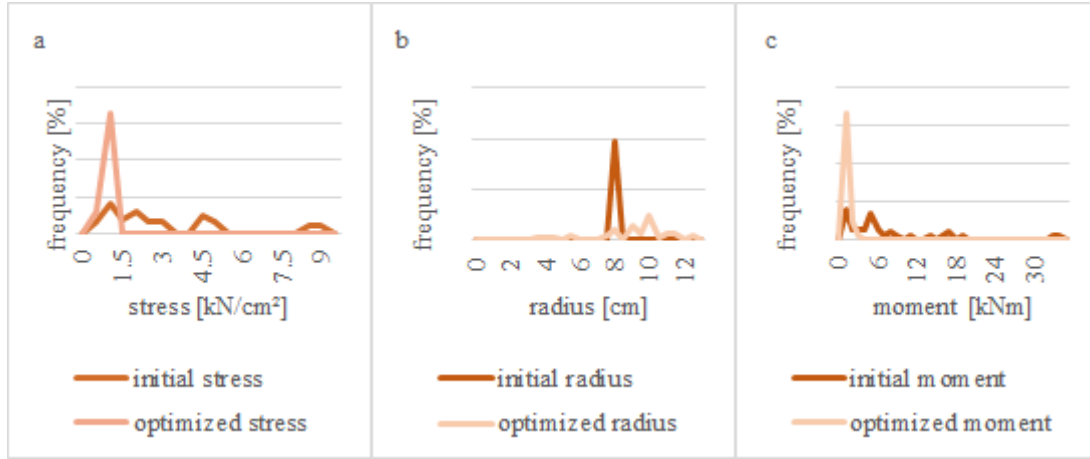

Figure 6. a: Distribution of stress within case study 1. b: Distribution of radii within case study 1. c: Distribution of moments within case study 1. measured at 40 probe points of the model.
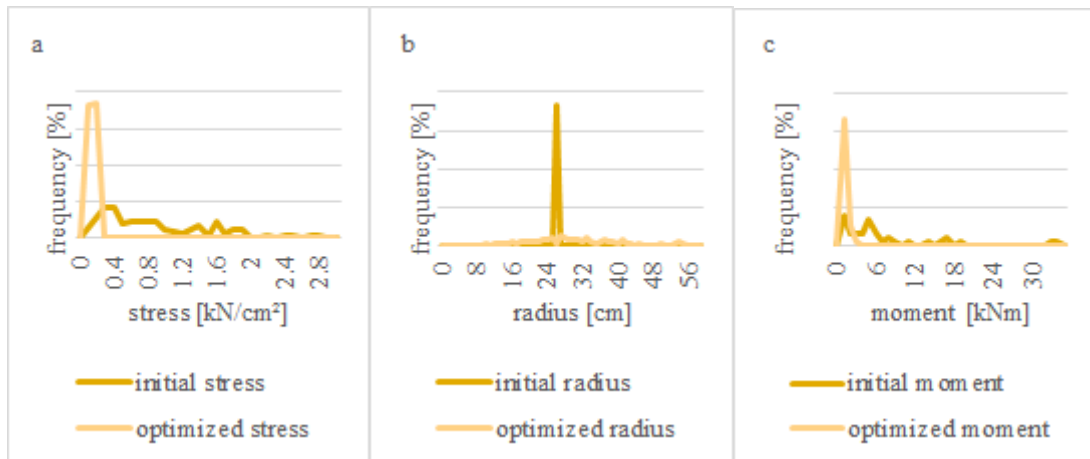

Figure 7. a: Distribution of stress within case study 2. b: Distribution of radii within case study 2. c: Distribution of moments within case study 2. measured at 368 probe points of the model.

4   CONCLUSION

The calculated equivalent stress (Figure 6a, Figure 7a) proves that the algorithm can achieve shape and size optimisation. When evaluating the resulting lattice structures (Figure 4, Figure 5), an adaptation along the tension and compression stress trajectories becomes apparent. Nevertheless, several possibilities to improve the algorithms' accuracy presented themselves while the research was conducted. Since the relationship between radius and volume in a cylinder

is not linear, altering the cross-sections by volume would be closer to natural ossification. A fixed overall volume during the simulation would mirror the reuse of bone tissue by real osteoblasts and osteoclasts. The consideration of torsion, shear forces, slenderness, and material strength in the calculation would increase the accuracy of the optimisation and would allow for material optimisation, targeting uniformly high utilisation grades just below 1.0 in all members.

Overall, the agent-based approach has several drawbacks. The artificial agents' limited vision, limited movement, and limited effect pose an additional processing layer and make it inferior to conventional structural optimisation methods, where the size and shape of the elements are the results of a direct calculation. Nonetheless, natural ossification cannot be described in a single optimal state but only as a process of successive actions of multiple agents influencing each other. This becomes evident by changing the starting point of a single agent, which has a non-linear impact and completely changes the structural outcome, resulting in a different local optimum. The initialisation parameters of the algorithm could provide an interesting vantage point for research into the conditions for bone homeostasis, e.g. implementing agent deactivation and activation and using genetic optimisation with the parameters in Table 1 as a gene pool. The agent-based system could be the conceptual ground for an algorithm using reinforcement learning, which, once trained, would reduce the computation time again for orders of magnitude. An agent-based system can serve as a theoretical basis for the realisation of adaptable load-bearing building structures. While the technology for its execution might not exist, the case of application does. The Python source code of the algorithm is publicly available at: https://github.com/rolfstarke/artificial-ossification

REFERENCES

Baumgartner, A., Harzheim, L., Mattheck, C., 1992. SK0 (soft kill option): the biological way to find an optimum structure topology 7.

Block, P., 2009. Thrust Network Analysis. Exploring three-dimensional equilibrium. PhD dissertation, Massachusetts Institute of Technology.

Block, P., Van Mele, T., Rippmann, M., Paulson, N., 2017, Beyond Bending. Reimagining compression shells, Munich: Edition Detail 2017. 64-75.

Boyle, C., Kim, I.Y., 2011. Three-dimensional micro-level computational study of Wolff's law via trabecular bone remodeling in the human proximal femur using design space topology optimization. Journal of Biomechanics 44, 935–942.

Cavazzuti, M., Baldini, A., Bertocchi, E., Costi, D., Torricelli, E., Moruzzi, P., 2011. High performance automotive chassis design: a topology optimization based approach. Struct Multidisc Optim 44, 45–56.

Hughes, T.J.R., 2000. The finite element method: linear static and dynamic finite element analysis. Dover Publications, Mineola, NY.

Jang, I.G., Kim, I.Y., 2008. Computational study of Wolff's law with trabecular architecture in the human proximal femur using topology optimization. Journal of Biomechanics 41, 2353–2361.

Januszkiewicz, K., Banachowicz, M., 2017. Nonlinear Shaping Architecture Designed with Using Evolutionary Structural Optimization Tools. IOP Conf. Ser.: Mater. Sci. Eng. 245, 082042.

Khurana, J.S., Safadi, F.F., 2010. Bone Structure, Development and Bone Biology, in: Essentials in Bone and Soft-Tissue Pathology. Springer US, Boston, MA, pp. 1–15.

Melcher, A., Vukorep, I., Hinze, T., 2019. Construction of Stable and Lightweight Technical Structures Inspired by Ossification of Bones Using Osteogenetic P Systems, in: Hinze, T., Rozenberg, G., Salomaa, A., Zandron, C. (Eds.), Membrane Computing. Springer Series Lecture Notes in Computer Science Vol. 11399, pp. 208–228.

Preisinger, C., 2013. Linking Structure and Parametric Geometry. Architectural Design 83, 110–113.

Safadi, F.F., Barbe, M.F., Abdelmagid, S.M., Rico, M.C., Aswad, R.A., Litvin, J., Popoff, S.N., 2009. Bone Structure, Development and Bone Biology, in: Khurana, J.S. (Ed.), Bone Pathology. Humana Press, Totowa, NJ, pp. 1–50.

Thiel, A., Reumann, M.K., Boskey, A., Wischmann, J., von Eisenhart-Rothe, R., Mayer-Kuckuk, P., 2018. Osteoblast migration in vertebrate bone. Biol Rev Camb Philos Soc 93, 350–363.

Van Lenthe, G.H., Stauber, M., Müller, R., 2006. Specimen-specific beam models for fast and accurate prediction of human trabecular bone mechanical properties. Bone 39, 1182–1189.

Weiner, S., Wagner, H.D., 1998. THE MATERIAL BONE: Structure-Mechanical Function Relations. Annu. Rev. Mater. Sci. 28, 271–298.

Wolff, 1892. Das Gesetz der Transformation der Knochen. Hirchwild, Berlin (Translated as The Law of Bone Remodeling. Springer, Berlin).